Quantum predator-prey cycles in dissipative Rydberg lattices

Ya-Xin Xiang,¹ Zhengyang Bai,^{1,*} and Yu-Qiang Ma^{1,2,†}

¹National Laboratory of Solid State Microstructures and School of Physics, Collaborative Innovation Center of Advanced Microstructures, Nanjing University, Nanjing 210093, China ²Hefei National Laboratory, Hefei 230088, China

The Lotka-Volterra model is a paradigm for self-organized predator-prey oscillations in far-from-equilibrium systems, yet testing it in real-world ecosystems is hindered by uncontrollable microscopic parameters. Here, we propose a quantum analogue of predator-prey dynamics using a tunable two-dimensional Rydberg atom array. Through mean-field analysis and numerical simulations based on the open-system discrete truncated Wigner approximation, we demonstrate that Rydberg excitations exhibit predator-prey cycles on microsecond timescales. We show that quantum coherence drives spontaneous symmetry breaking, while long-range interactions stabilize global oscillations against quantum-noise-induced desynchronization. We further reveal that quantum jump induce quasicycles whose amplitude scales inversely with the square root of the system size. Our work extends the study of predator-prey models to the quantum realm and advances quantum simulation stratagies that leverage engineered many-body nonequilibrium effects.

Introduction.—The Lotka–Volterra model uses deterministic equations to describe the cyclic dynamics of predator—prey ecosystems [1, 2]. As an exemplar of self-organization far from equilibrium, it shows how simple local interactions can produce emergent oscillations, inspiring studies of spontaneous oscillations across diverse fields, including chemical reactions [3–6], biological rhythms [7–9], epidemic spread [10–12], and evolutionary game theory [13–15]. To reflect real-world complexity, stochastic lattice Lotka–Volterra model were developed, uncovering rich noise-induced effects [16–20]. However, empirical validation in natural ecosystems remains challenging, as key parameters like reproduction rates and mobility are difficult to measure or control.

Recently, cold-atom systems excited to high-lying Rydberg states have emerged as a powerful platform for investigating nonequilibrium quantum many-body dynamics [21–26]. In particular, Rydberg atoms in optical tweezer arrays offer single-atom control and scalability, making them ideal for quantum simulation and computation [27–31]. The strong and programmable Rydberg-Rydberg interactions drive a rich array of self-organization phenomena [32–40], enabling a bottom-up understanding of how macroscopic collective behavior originate from microscopic interactions.

Here, we demonstrate the emergence of predator-prey cycles in a two-component two-dimensional (2D) Rydberg atom array, as schematized in Figs. 1(a) and (b). The predator-prey limit cycle (LC) manifests as periodic out-of-phase oscillation between one component ($|s\rangle$, predator) and the other ($|r\rangle$, prey) and evolves through three distinct dynamical states: (I) prey accumulation, (II) subsequent predator growth, and (III) suppression of both [see Figs. 1(c) and (d)]. Crucially, these LCs emerge exclusively in the quantum regime without classical counterparts, as dynamics of quantum coherence is

indispensable for breaking the time-translation symmetry.

Using the open-system discrete truncated Wigner approximation (OSDTWA), we also reveal quantum-jump-induced quasicycles whose oscillation amplitude scales inversely with the square root of the system size. Notably, these quantum quasicycles exhibit frequencies distinct from their classical counterparts [16, 17], suggesting a fundamentally different microscopic mechanism for noise amplification. Parallel to the absence of synchronization and global oscillations observed in classical stochastic lat-

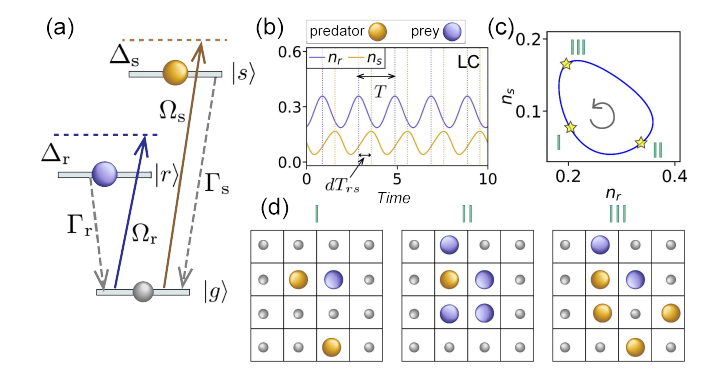


FIG. 1. (a) The three-level scheme. The ground state $|q\rangle$ is coupled to the Rydberg states $|s\rangle$ and $|r\rangle$ by a laser field. Excited atoms in the state $|s\rangle$ ($|r\rangle$) decay to the ground state at rates Γ_r (Γ_s). Mean-field analysis reveals (b) predator-prey dynamics with alternating dominance between $|r\rangle$ (preys) and $|s\rangle$ (predators) populations characterized with period $T \approx 2/\Gamma_r$ and relative time advance dT_{rs} of peaks in n_r (yellow dotted lines) over peaks in n_s (purple dotted lines), manifesting a (c) limit cycle (LC) in the n_s - n_r phase space with (d) three distinct dynamical phases emerging subsequently: In phase I, low excited populations favor $|g\rangle \rightarrow |r\rangle$ transition, while interaction-induced level shifts suppress $|g\rangle \rightarrow |s\rangle$ transition. In phase II, high n_r enhances $|g\rangle \rightarrow |s\rangle$ transition and suppress $|g\rangle \rightarrow |r\rangle$ transition. In phase III, both excitation processes are blocked and the system returns to the low-excitation phase I.

^{*} zhybai@nju.edu.cn

[†] myqiang@nju.edu.cn

tice systems [41], our simulations reveal that in large systems with finite-range van der Waals (vdW) interactions, local quantum jumps induce significant desynchronization. Consequently, within the LC regime, global oscillations are significantly suppressed, and their amplitude decreases with increasing system sizes.

Model.—We study a spin-1 model for a dissipative Rydberg gas, as illustrated in Fig. 1(a). It comprises N atoms arranged in a 2D lattice where the ground state $|g\rangle$ is coupled to two highly-excited Rydberg levels $|r\rangle$, $|s\rangle$ by lasers with Rabi frequencies Ω_r , Ω_s and detuning Δ_r , Δ_s from resonance. Upon excitation, the Rydberg states $|r\rangle$ and $|s\rangle$ interact via strong and long-range interactions.

This system permits a microscopic description via a quantum master equation for the many-body density operator $\hat{\rho}$ ($\hbar = 1$ hereinafter),

$$\partial_t \hat{\rho} = i \left[\hat{\rho}, \hat{H} \right] + \hat{D}[\hat{\rho}] \tag{1}$$

where the Hamiltonian \hat{H} responsible for the coherent dynamics reads

$$\hat{H} = \sum_{l=1}^{N} \left[\left(\frac{\Omega_s}{2} \hat{\sigma}_l^{gs} + \frac{\Omega_r}{2} \hat{\sigma}_l^{gr} + \text{h.c.} \right) - \Delta_r \hat{\sigma}_l^{rr} - \Delta_s \hat{\sigma}_l^{ss} \right]$$

$$+ \sum_{l,k \neq l} \left(V_{lk,ss} \hat{\sigma}_k^{ss} + V_{lk,sr} \hat{\sigma}_k^{rr} \right) \hat{\sigma}_l^{ss}$$

$$+ \sum_{l,k \neq l} \left(V_{lk,rr} \hat{\sigma}_k^{rr} + V_{lk,sr} \hat{\sigma}_k^{ss} \right) \hat{\sigma}_l^{rr}$$

$$(2)$$

where h.c. stands for Hermitian conjugation, and l,k denotes atomic sites and the transition operator $\hat{\sigma}_l^{ab} \equiv |a\rangle_l \, \langle b|_l$ for a,b=g,s,r, and the interactions between Rydberg states $|a\rangle$ and $|b\rangle$ are parameterized by $V_{lk,ab}$. The dissipative dynamics arising from spontaneous decay of the Rydberg states $|r\rangle$ and $|s\rangle$ to the ground state is described by $\hat{\boldsymbol{D}}[\hat{\rho}] = \sum_{l,a=s,r} \Gamma_a \, (\hat{\sigma}_l^{ga} \, \hat{\rho} \hat{\sigma}_l^{ag} - \{\hat{\sigma}_l^{aa}, \hat{\rho}\}/2)$ with the decay rate Γ_a .

To characterize the dynamical behavior of the system, we begin with a mean-field (MF) ansatz by assuming that the total density matrix factorizes as $\hat{\rho} = \prod_l \hat{\rho}_l$, with interactions treated via a MF coupling (a,b=s,r) $\chi_{ab} = 2N^{-1}\sum_{k\neq l}V_{lk,ab}$. The phase diagram is determined by the fixed points in the equations of motion for the expectation values $\sigma^{ab} = N^{-1}\sum_l \langle \hat{\sigma}_l^{ab} \rangle$ and the eigenvalues of their corresponding 8×8 Jacobian. The two-component Rydberg populations are denoted by $n_a=\sigma^{aa}$. Throughout this study, we adopt a parameter set with $\Gamma_s=\Gamma_r=\Gamma=1,\,\Omega_s=\Omega_r=\Omega,\,\Delta_s=8,$ and $\chi_{ab}=\chi=12,$ without loss of generality.

The eigenvalues, displayed as complex conjugate pairs and sorted by their real parts $\Re[\lambda_0] \geq \Re[\lambda_1] \geq ...$ are shown in Figs. 2(a) and (b). The real and imaginary parts of λ_0 govern the relaxation timescale and oscillation frequency of fluctuations near the fixed point, respectively. A fixed point is linearly stable if $\Re[\lambda_0] < 0$ and

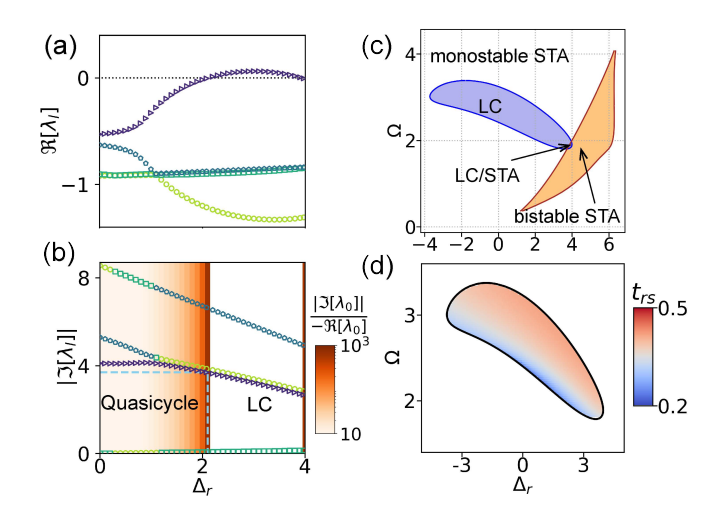


FIG. 2. Mean-field analysis. (a) Real and (b) imaginary parts of the Jacobian eigenvalues λ_l . Quasicycles occur when the ratio (color-coded) $-|\Im[\lambda_0]|/\Re[\lambda_0]\gg 0$. In panel (b), the blue dashed lines mark a quasicycle at $\Delta_r=2.1$ with frequency ≈ 3.7 . Eigenvalues are conjugate pairs sorted by real parts in decending order. (c) Phase diagram in Ω - Δ_r parameter space showing monostable stationary (STA), purely LC, STA/LC coexistence, and bistable STA phases. (d) Normalized time advance $t_{rs}=dT_{rs}/T$ of LC, where dT_{rs} is the time advance of n_r peaks relative to n_s and T is the period. Parameters for (a)(b): $\Omega=2$.

unstable if $\Re[\lambda_0] > 0$. For small values of the detuning Δ_r , a stable fixed point occurs. Notably, the real parts of the dominant eigenvalue pair λ_0, λ_0^* increase with Δ_r , transitioning from negative to positive values [Fig. 2(a)], signifying a dynamic phase transition from a stationary state to a LC state. Near this transition, quasicycles also arise when $-|\Im[\lambda_0]|/\Re[\lambda_0] \gg 1$ [Fig. 2(b)].

The phase diagram spanned by Ω and Δ_r features four distinct regimes: monostable stationary state, purely LC state, coexistence between two stationary states and a LC state, and bistable stationary states [Fig. 2(c)]. In the LC region, the oscillation occurs with a period on the order of microseconds, set by the atomic decay rate [21, 23]. The emergent predator-prey cycles are characterized by the normalized time advance $t_{rs} = dT_{rs}/T$ [see Fig. 1(b)], representing the relative timing between peaks in n_s and n_r within an oscillation period T. Owing to the periodicity of the oscillations, t_{rs} is constrained to the interval [-0.5, 0.5). A value of $t_{rs} = 0$ corresponds to synchronization between the two Rydberg components, while positive values in the range $t_{rs} \in (0.2, 0.5)$ [see Fig. 2(d) indicate a predator-prey dynamic in which the state $|s\rangle$ atoms act as the predators that feed on the state $|r\rangle$ atoms. This predator-prey role is reversed upon the exchange of detunings $\Delta_r \leftrightarrow \Delta_s$.

To isolate the role of quantum coherence, we study a classical regime where all off-diagonal elements of the density operator are adiabatically eliminated, yielding a 2×2 Jacobian [22, 42]. The resulting Jacobian has purely real, negative eigenvalues [see Sec. I of the Supplementary

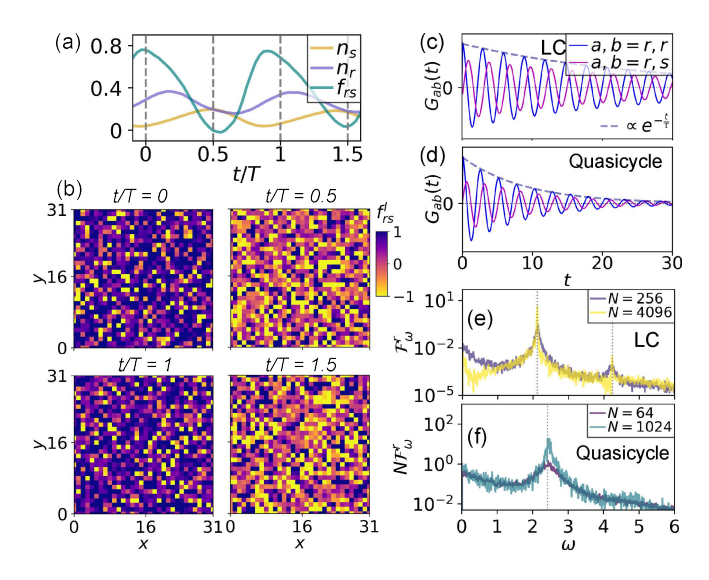


FIG. 3. Results from OSDTWA with all-to-all coupling on a 2D lattice. (a) Time series of average Rydberg population n_s, n_r for both components, and the relative faction $f_{rs} = (n_r - n_s)/(n_r + n_s)$ for LC. Time is rescaled by the period T measured from the time series, and the vertical dashed gray lines stand for half-period intervals, with the corresponding spatial profile of f_{rs}^l shown in (b). $f_{rs} = 1$ stands for $n_s = 1$ $0, n_r = 1$, while $f_{rs} = -1$ corresponds to $n_s = 1, n_r = 0$. The auto-correlation function $G_{rr}(t) = \langle \delta n_r(t') \delta n_r(t'+t) \rangle_{t'}$, and the cross-correlation function $G_{rs}(t) = \langle \delta n_r(t') \delta n_s(t'+t) \rangle_{t'}$ with $\delta n_{r,s} = n_{r,s} - \langle n_{r,s} \rangle_t$ for N = 256 for (c) LC and (d) quasicycle. The characteristic lifetime τ is obtained from fitting the peak-envelope to $Ae^{-t/\tau}$ (gray dashed lines). The Fourier spectra for (e) LC and (f) quasicycles (rescaled by system size N). The intrinsic frequency is marked by gray dotted lines. Parameters for (a)-(c)(e): $\Delta_r = 3$; parameters for (d)(f): $\Delta_r = 2.1$. Correlation functions are averaged over trajectories of duration $\geq 10^4$ for well-converged statistics.

Material (SM)], indicating that both LC and quasicycles are entirely absent in the classical regime.

2D Rydberg lattice—To go beyond the MF theory, we employ OSDTWA to simulate stochastic spin-1 Rydberg array system. This approach combines the semiclassical framework of the discrete truncated Wigner approximation with the method of quantum jumps [43, 44] [see Sec.II of SM for details]. The atoms are arranged on a 2D square lattice comprising $N=L^2$ sites with a unit spacing, and edge length L, where each site is occupied by a single atom, consistent with experimental realizations [32, 33, 45].

We begin with all-to-all coupling where each Rydberg atom interacts with a collective field generated by all other Rydberg atoms. This approximation suppresses atom-to-atom fluctuations, leaving finite-size fluctuations as the primary correction to the systemic dynamics. Within the parameter regime for MF LC, the average Rydberg population (a=r,s) $n_a=\langle n_a^l\rangle_l$ for both components evolve periodically with time [Fig. 3(a)]. To further quantify the predator-prey dynamics, we introduce the relative fraction $f_{rs}^l=(n_r^l-n_s^l)/(n_r^l+n_s^l)$,

 $f_{rs} = \langle f_{rs}^l \rangle_l$, where $f_{rs} > 0$ corresponds to dominance of the r-component atoms and $f_{rs} < 0$ indicates dominance of the s-component atoms. For a system with N=1024 atoms, f_{rs} oscillates between 0 and 0.8 [Fig. 3(a)], confirming the emergence of predator-prey dynamics in the two-component Rydberg lattice. As evidenced by the alternating spatial profile of f_{rs}^l within the array [Fig. 3(b)], local quantum jumps produce significant atom-to-atom fluctuations, analogous to spatiotemporal patterns in classical predator-prey systems [46].

To pinpoint the predator-prey dynamics, we introduce the two-time correlation functions [23] (a, b = r, s).

$$G_{ab}(t) = \langle \delta n_a(t') \delta n_b(t+t') \rangle_{t'} \tag{3}$$

where $\delta n_a = n_a - \langle n_a \rangle_t$ and their Fourier components $\mathcal{F}^a_\omega = \int d\omega G_{aa}(t) e^{i\omega t}$. For auto correlations $G_{aa}(t)$, the first peak always occurs at t=0. In contrast, for cross correlations $G_{ab}(t), a \neq b$, the first peak may occur at a finite time delay $t \in (0, T/2]$. This corresponds to a relative time advance of the peaks in the a-component with respect to those in the b-component, manifesting as a phase shift characteristic of a predator-prey relation.

This behavior is confirmed with the oscillating auto-correlation function G_{rr} and cross-correlation function G_{rs} displayed in Fig. 3(c). The coherence time τ characterizes the decay of the envelope. The first peak of G_{rs} locates at finite time delay t indicates a phase shift between r- and s-components, consistent with the MF results shown in Fig. 2(d). These oscillatory auto-correlation functions give rise to peaks in the Fourier components \mathcal{F}^r_{ω} at integer multiples of the intrinsic frequency, as depicted in Fig. 3(e).

The separation of relaxation and oscillation timescales, governed by the real and imaginary parts of the eigenvalues [see Figs. 2(a) and (b)], indicates that finite-size noise can induce quasicycles in a stable steady state. This occurs when $|\Im[\lambda_0]| \gg -\Re[\lambda_0] > 0$, a condition satisfied by tuning the detuning parameter Δ from 3 to 2.1, which increases $|\Im[\lambda_0]|$ and drives the transition from a LC to a quasicycle state. The scaled Fourier components $N\mathcal{F}^r_{\omega}$ are displayed in Fig. 3(f). The data collapse for different system sizes confirms that quantum quasicycles exhibit amplitude scaling $\delta n_{s,r} \propto 1/\sqrt{N}$, consistent classical quasicycles [17, 47-49]. Meanwhile, we observe an intrinsic frequency $[\omega \approx 2.4]$, indicated by the gray dotted line that is distinct from the one induced by Gaussian noise $[\Im[\lambda_0] \approx 3.7$ indicated by the blue lines in Fig. 2(b)]. This difference arises from quantum fluctuations, a feature that underscores a different mechanism of noise amplification.

Similar to LC, quasicycles exhibit a non-zero phase shift between the two components [Fig. 3(d)], indicating that quantum fluctuations preserve the predator-prey relation of LCs. However, unlike quasicycles, LCs lack the characteristic $1/\sqrt{N}$ scaling [Figs. 3(e) and (f)]. Their Fourier spectra instead exhibit distinct peaks at integer multiples of the intrinsic frequency [dotted lines in

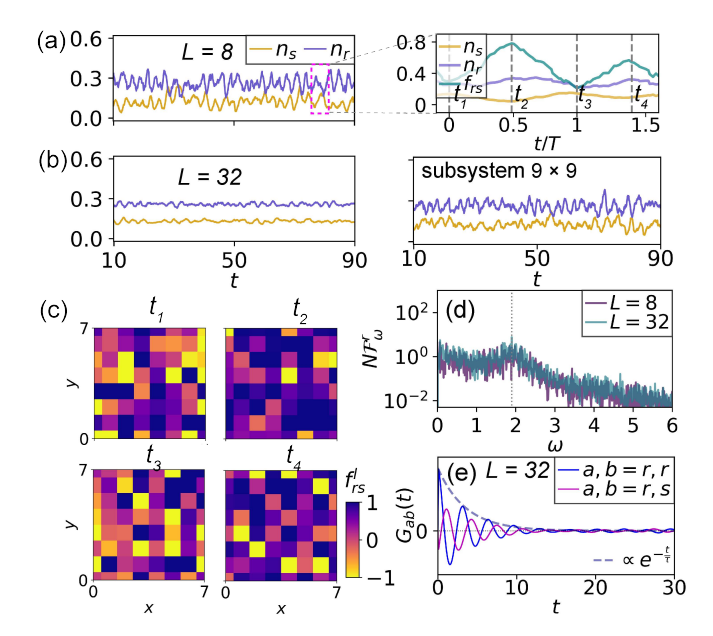


FIG. 4. Results from OSDTWA with vdW coupling on a 2D lattice of edge length L. (a) Time series of average Rydberg population n_s and n_r for a small system (L=8). Left: full time series, right: zoom-in view, with corresponding spatial profile of the relative fraction f_{rs}^l shown in (c) and dashed lines marking the snapshots times. (b) Time series for a large system (L=32). Left: whole system, right: a subsystem with edge length 9. (d) Fourier components of G_{rr} (rescaled by system size $N=L^2$) for small and large systems. Dashed line indicates oscillation frequency. (e) Two-time auto-correlation G_{rr} and cross-correlation G_{rs} . Parameters for (a)-(g): $\Delta_r=3$.

Fig. 3(e)], indicative of time-translation symmetry breaking, consistent with behavior in the thermodynamic limit.

The all-to-all coupling stabilizes global oscillations against atom-to-atom fluctuations induced by quantum jumps. This contrasts sharply with systems governed by finite-range vdW interactions, where local fluctuations cause desynchronization. Consequently, global oscillations in the average Rydberg populations n_s and n_r are more pronounced in smaller systems (L = 8) than in larger ones (L = 32), as shown in Figs. 4(a) and (b). In small systems (L=8), short-time cyclic dynamics [right panel of Fig. 4(a)] and an alternating spatial profile in relative faction f_{rs}^l [Fig. 4(c)] occur. However, the oscillation amplitude scales inversely with the square root of the system size [Fig. 4(d)], and oscillations persist only in local subsystems of large arrays [right panel of Fig. 4(b)]. These demonstrate a lack of global synchronization in large systems, mirroring earlier findings in stochastic reaction-diffusion lattice systems [41, 50].

Although global oscillations are significantly suppressed in larger systems, where individual trajectories resemble a stochastic steady state [see left panel of Fig. 4(b)]. The hidden predator–prey relation is revealed in the two-time cross-correlation functions $G_{rs}(t)$. As evidenced in Fig. 4(e), these correlation functions ex-

hibit a phase shift and the intrinsic frequency characteristic of predator-prey dynamic in their short-time dynamics. However, the long-time periodicity is significantly disrupted by quantum-jump induced desynchronization, merging the several sharp Fourier peaks [Fig. 3(e)] into a single broadened feature [Fig. 4(d)].

Conclusion and Discussion.—In this work, we demonstrate the rise of emergent predator-prey cycles in a driven-dissipative two-component atomic array. While the Lotka-Volterra model for predator-prey dynamics is a paradigm for self-organization far from equilibrium, testing it with uncontrolled natural ecosystems is difficult. By establishing the explicit connections between microscopic parameters, such as laser detuning, Rabi frequencies, and atomic interaction strength, and the emergent properties (frequency and phase shift) of the predator-prey cycles, our work positions the two-component Rydberg atomic lattices as a highly controllable experimental platform for exploring self-organizing phenomena in nonequilibrium systems

In classical population dynamics, finite-system effects are typically introduced via multiplicative white Gaussian noises, which induce various noise-induced phenomena absent in MF models [51–56]. Here, prior to the onset of the LC phase, our system exhibits quasicycles driven by the amplification of intrinsic quantum noises from quantum jumps. As finite-size effects, these quantum quasicycles are expected to disappear in the thermodynamic limit. Crucially, unlike their classical counterparts [17], they exhibit a distinct intrinsic frequency not captured by Gaussian-noise approximations.

By comparing systems with all-to-all and short-range vdW coupling, we identify long-range interactions as a crucial mechanism for stabilizing global oscillations against local quantum jumps. The inverse square-root scaling of the oscillation amplitude with system sizes and the presence of oscillatory subsystems show that large systems comprise independent oscillating parts [50]. This contrasts sharply with global oscillatory states driven by self-organized bistability, where dissipative first-order phase transitions induce transient long-range correlations through system-spanning avalanches [57].

Of particular relevance to this context, Jiao et al. recently observed predator–prey dynamics in a thermal Rydberg vapor system [58]. In their experiment, strong dephasing and ionization of Rydberg atoms in a room-temperature vapor cell lead to a purely dissipative and incoherent coupling between atoms and ions, mediated by external laser fields. Our findings highlight the crucial role of nonperturbative quantum coherence in breaking continuous time-translation symmetry and generating such periodic cycles.

ACKNOWLEDGMENTS

We are deeply grateful to U. C. Täuber for his insightful suggestions. This work is supported by the Na-

tional Natural Science Foundation of China under Grants No. 12274131, No. 12347102 and No. 12174184, the Natural Science Foundation of Jiangsu Province under Grant No. BK20233001, and the Innovation Program

for Quantum Science and Technology under Grant No. 2024ZD0300101. The authors also acknowledge the computational resources provided by the High Performance Computing Center of Nanjing University.

- [1] V. Volterra, Fluctuations in the abundance of a species considered mathematically, Nature 118, 558 (1926).
- [2] A. J. Lotka, Analytical note on certain rhythmic relations in organic systems, Proc. Natl. Acad. Sci. U. S. A. 6, 410 (1920).
- [3] W. C. Bray, A periodic reaction in homogeneous solution and its relation to catalysis, J. Am. Chem. Soc. 43, 1262 (1921).
- [4] I. Prigogine and R. Lefever, Symmetry breaking instabilities in dissipative systems. II, J. Chem. Phys. 48, 1695 (1968).
- [5] R. Lefever and G. Nicolis, Chemical instabilities and sustained oscillations, J. Theor. Biol. 30, 267 (1971).
- [6] A. Zhabotinsky and A. Zaikin, Autowave processes in a distributed chemical system, J. Theo. Biol. 40, 45 (1973).
- [7] J. J. Tyson, K. C. Chen, and B. Novak, Sniffers, buzzers, toggles and blinkers: dynamics of regulatory and signaling pathways in the cell, Curr. Opin. Cell Biol. 15, 221 (2003).
- [8] J. J. Tyson, K. Chen, and B. Novak, Network dynamics and cell physiology, Nat. Rev. Mol. Cell Biol. 2, 908 (2001).
- [9] A. Goldbeter, Computational approaches to cellular rhythms, Nature 420, 238 (2002).
- [10] M. S. Bartlett, Measles periodicity and community size, J. R. Stat. Soc. Ser. A (Gen.) 120, 48 (1957).
- [11] M. Greer, R. Saha, A. Gogliettino, C. Yu, and K. Zollo-Venecek, Emergence of oscillations in a simple epidemic model with demographic data, R. Soc. Open Sci. 7, 191187 (2020).
- [12] H. W. Hethcote and S. A. Levin, Periodicity in epidemiological models, in *Applied Mathematical Ecology*, edited by S. A. Levin, T. G. Hallam, and L. J. Gross (Springer Berlin Heidelberg, Berlin, Heidelberg, 1989) pp. 193–211.
- [13] K. Sigmund, Oscillations in the evolution of reciprocity, J. Theo. Biol. 137, 21 (1989).
- [14] B. Sinervo and C. M. Lively, The rock-paper-scissors game and the evolution of alternative male strategies, Nature 380, 240 (1996).
- [15] A. Roman, D. Dasgupta, and M. Pleimling, Interplay between partnership formation and competition in generalized May-Leonard games, Phys. Rev. E 87, 032148 (2013).
- [16] M. Mobilia, I. T. Georgiev, and U. C. Täuber, Phase transitions and spatio-temporal fluctuations in stochastic lattice Lotka–Volterra models, Journal of Statistical Physics 128, 447 (2007).
- [17] A. J. McKane and T. J. Newman, Predator-prey cycles from resonant amplification of demographic stochasticity, Phys. Rev. Lett. 94, 218102 (2005).
- [18] U. C. Täuber, Stochastic population oscillations in spatial predator-prey models, in *J. Phys. Conf. Ser.*, Vol. 319 (IOP Publishing, 2011) p. 012019.
- [19] T. Antal and M. Droz, Phase transitions and oscillations in a lattice prey-predator model, Phys. Rev. E 63, 056119

- (2001).
- [20] J. E. Satulovsky and T. Tomé, Stochastic lattice gas model for a predator-prey system, Phys. Rev. E 49, 5073 (1994).
- [21] N. Šibalic and C. S. Adams, Rydberg Physics, 2399-2891 (IOP Publishing, 2018).
- [22] S. Helmrich, A. Arias, G. Lochead, T. M. Wintermantel, M. Buchhold, S. Diehl, and S. Whitlock, Signatures of self-organized criticality in an ultracold atomic gas, Nature 577, 481 (2020).
- [23] X. Wu, Z. Wang, F. Yang, R. Gao, C. Liang, M. K. Tey, X. Li, T. Pohl, and L. You, Dissipative time crystal in a strongly interacting Rydberg gas, Nat. Phys. 20, 1389 (2024).
- [24] D. Ding, Z. Bai, Z. Liu, B. Shi, G. Guo, W. Li, and C. S. Adams, Ergodicity breaking from Rydberg clusters in a driven-dissipative many-body system, Sci. Adv. 10, eadl5893 (2024).
- [25] K. Wadenpfuhl and C. S. Adams, Emergence of synchronization in a driven-dissipative hot Rydberg vapor, Phys. Rev. Lett. 131, 143002 (2023).
- [26] D.-S. Ding, H. Busche, B.-S. Shi, G.-C. Guo, and C. S. Adams, Phase diagram and self-organizing dynamics in a thermal ensemble of strongly interacting Rydberg atoms, Phys. Rev. X 10, 021023 (2020).
- [27] H. Weimer, M. Müller, I. Lesanovsky, P. Zoller, and H. P. Büchler, A Rydberg quantum simulator, Nat. Phys. 6, 382 (2010).
- [28] A. Browaeys and T. Lahaye, Many-body physics with individually controlled Rydberg atoms, Nat. Phys. 16, 132 (2020).
- [29] M. Saffman, T. G. Walker, and K. Mølmer, Quantum information with Rydberg atoms, Rev. Mod. Phys. 82, 2313 (2010).
- [30] R. Lin, H.-S. Zhong, Y. Li, Z.-R. Zhao, L.-T. Zheng, T.-R. Hu, H.-M. Wu, Z. Wu, W.-J. Ma, Y. Gao, Y.-K. Zhu, Z.-F. Su, W.-L. Ouyang, Y.-C. Zhang, J. Rui, M.-C. Chen, C.-Y. Lu, and J.-W. Pan, AI-enabled parallel assembly of thousands of defect-free neutral atom arrays, Phys. Rev. Lett. 135, 060602 (2025).
- [31] C. Chen, G. Emperauger, G. Bornet, F. Caleca, B. Gély, M. Bintz, S. Chatterjee, V. Liu, D. Barredo, N. Y. Yao, T. Lahaye, F. Mezzacapo, T. Roscilde, and A. Browaeys, Spectroscopy of elementary excitations from quench dynamics in a dipolar xy rydberg simulator, Science 389, 483 (2025).
- [32] S. Ebadi, T. T. Wang, H. Levine, A. Keesling, G. Semeghini, A. Omran, D. Bluvstein, R. Samajdar, H. Pichler, W. W. Ho, et al., Quantum phases of matter on a 256-atom programmable quantum simulator, Nature 595, 227 (2021).
- [33] E. Guardado-Sanchez, P. T. Brown, D. Mitra, T. Devakul, D. A. Huse, P. Schauß, and W. S. Bakr, Probing the quench dynamics of antiferromagnetic correlations in a 2d quantum Ising spin system, Phys. Rev. X 8, 021069

- (2018).
- [34] G. Semeghini, H. Levine, A. Keesling, S. Ebadi, T. T. Wang, D. Bluvstein, R. Verresen, H. Pichler, M. Kalinowski, R. Samajdar, et al., Probing topological spin liquids on a programmable quantum simulator, Science 374, 1242 (2021).
- [35] H. Bernien, S. Schwartz, A. Keesling, H. Levine, A. Omran, H. Pichler, S. Choi, A. S. Zibrov, M. Endres, M. Greiner, et al., Probing many-body dynamics on a 51-atom quantum simulator, Nature 551, 579 (2017).
- [36] X. Liang, Z. Yue, Y.-X. Chao, Z.-X. Hua, Y. Lin, M. K. Tey, and L. You, Observation of anomalous information scrambling in a rydberg atom array, Phys. Rev. Lett. 135, 050201 (2025).
- [37] L. Li, D.-S. Xiang, Y.-W. Zhang, H.-X. Liu, P. Zhou, D. Yuan, K. Zhang, S.-Y. Zhang, B. Xu, L. Liu, and Y. Li, Observation of quantum information collapse-andrevival in a strongly-interacting Rydberg atom array (2024).
- [38] T. Manovitz, S. H. Li, S. Ebadi, R. Samajdar, A. A. Geim, S. J. Evered, D. Bluvstein, H. Zhou, N. U. Koyluoglu, J. Feldmeier, et al., Quantum coarsening and collective dynamics on a programmable simulator, Nature 638, 86 (2025).
- [39] V. Lienhard, S. de Léséleuc, D. Barredo, T. Lahaye, A. Browaeys, M. Schuler, L.-P. Henry, and A. M. Läuchli, Observing the space- and time-dependent growth of correlations in dynamically tuned synthetic ising models with antiferromagnetic interactions, Phys. Rev. X 8, 021070 (2018).
- [40] A. Keesling, A. Omran, H. Levine, H. Bernien, H. Pichler, S. Choi, R. Samajdar, S. Schwartz, P. Silvi, S. Sachdev, et al., Quantum kibble–zurek mechanism and critical dynamics on a programmable Rydberg simulator, Nature 568, 207 (2019).
- [41] F. Baras, Stochastic analysis of limit cycle behavior in spatially extended systems, Phys. Rev. Lett. 77, 1398 (1996).
- [42] I. Lesanovsky and J. P. Garrahan, Kinetic Constraints, Hierarchical Relaxation, and Onset of Glassiness in Strongly Interacting and Dissipative Rydberg Gases, Phys. Rev. Lett. 111, 215305 (2013).
- [43] V. P. Singh and H. Weimer, Driven-dissipative criticality within the discrete truncated Wigner approximation, Phys. Rev. Lett. 128, 200602 (2022).
- [44] B. Zhu, A. M. Rey, and J. Schachenmayer, A generalized

- phase space approach for solving quantum spin dynamics, New J. Phys. **21**, 082001 (2019).
- [45] H. J. Manetsch, G. Nomura, E. Bataille, X. Lv, K. H. Leung, and M. Endres, A tweezer array with 6100 highly coherent atomic qubits, Nature 10.1038/s41586-025-09641-4 (2025).
- [46] U. C. Täuber, Stochastic Spatial Lotka-Volterra Predator-Prey Models, in *Order*, *Disorder and Criticality* (WORLD SCIENTIFIC, 2024) pp. 67–115.
- [47] P. C. Bressloff, Metastable states and quasicycles in a stochastic Wilson-Cowan model of neuronal population dynamics, Phys. Rev. E 82, 051903 (2010).
- [48] A. J. McKane, J. D. Nagy, T. J. Newman, and M. O. Stefanini, Amplified biochemical oscillations in cellular systems, J. Stat. Phys. 128, 165 (2007).
- [49] R. P. Boland, T. Galla, and A. J. McKane, How limit cycles and quasi-cycles are related in systems with intrinsic noise, J. Stat. Mech. 2008, P09001 (2008).
- [50] U. Dobramysl, M. Mobilia, M. Pleimling, and U. C. Täuber, Stochastic population dynamics in spatially extended predator-prey systems, J. Phys. A Mathe. Theo. 51, 063001 (2018).
- [51] T. Tomé and M. J. de Oliveira, Role of noise in population dynamics cycles, Phys. Rev. E 79, 061128 (2009).
- [52] T. Biancalani, L. Dyson, and A. J. McKane, Noiseinduced bistable states and their mean switching time in foraging colonies, Phys. Rev. Lett. 112, 038101 (2014).
- [53] C. F. Lee, Predicting rare events in chemical reactions: Application to skin cell proliferation, Phys. Rev. E 82, 021103 (2010).
- [54] T. Biancalani, T. Rogers, and A. J. McKane, Noiseinduced metastability in biochemical networks, Phys. Rev. E 86, 010106 (2012).
- [55] T. Biancalani, F. Jafarpour, and N. Goldenfeld, Giant amplification of noise in fluctuation-induced pattern formation, Phys. Rev. Lett. 118, 018101 (2017).
- [56] D. Karig, K. M. Martini, T. Lu, N. A. DeLateur, N. Gold-enfeld, and R. Weiss, Stochastic Turing patterns in a synthetic bacterial population, Proc. Natl. Acad. Sci. U. S. A. 115, 6572 (2018).
- [57] Y.-X. Xiang, Q.-L. Lei, Z. Bai, and Y.-Q. Ma, Self-organized time crystal in driven-dissipative quantum system, Phys. Rev. Res. 6, 033185 (2024).
- [58] Y. Jiao, Y. Zhang, J. Bai, W. Jiang, Y. He, H. Shen, S. Jia, J. Zhao, and C. S. Adams, Quantum Lotka-Volterra dynamics (2024), arXiv:2408.01726 [quant-ph].